

**Pair-density wave signature observed by x-ray scattering in  
La-based high- $T_c$  cuprates**

Jun-Sik Lee,<sup>1,\*</sup> Steven A. Kivelson,<sup>2</sup> Tong Wang,<sup>3</sup> Yoichi Ikeda,<sup>3</sup>

Takanori Taniguchi,<sup>3</sup> Masaki Fujita,<sup>3</sup> and Chi-Chang Kao<sup>4</sup>

<sup>1</sup>*Stanford Synchrotron Radiation Lightsource,*

*SLAC National Accelerator Laboratory,*

*Menlo Park, California 94025, USA*

<sup>2</sup>*Departments of Physics, Stanford University, Stanford, CA 94305, USA*

<sup>3</sup>*Institute for Materials Research, Tohoku University,*

*Katahira 2-1-1, Sendai, 980-8577, Japan*

<sup>4</sup>*SLAC National Accelerator Laboratory,*

*Menlo Park, California 94025, USA*

Suggestive, but indirect evidence of the existence of pair-density wave (PDW) order in several high- $T_c$  cuprates has been reported [1–13]. As this constitutes a new quantum phase of matter, it is important to *establish* its existence at least somewhere in the phase diagram [14–17]. However, a direct correspondence between experiment [1–13, 18–23] and theory [24–35] has remained elusive. Here, we report the observation of a theoretically predicted PDW *bulk* signature in two La-based cuprates, Sr-doped  $\text{La}_{1.875}\text{Ba}_{0.125}\text{CuO}_4$  and Fe-doped  $\text{La}_{1.87}\text{Sr}_{0.13}\text{CuO}_4$ , through a comprehensive study that incorporates zero-magnetic field x-ray scattering, neutron scattering, and transport measurements. Specifically, we observe the emergence of so-called “1Q” order, which is to say subharmonic order associated with the charge-density wave (CDW) stripes, in a range of temperatures in which independent evidence suggests the co-existence of PDW long-range order and fluctuating uniform superconducting order. The subharmonic order is most pronounced around a half-integer  $l$ -vector, where the CDW diffraction peak is also strongest. This is consistent with the theoretical proposal [24–27] that the cancellation of the Josephson coupling (“layer-decoupling”), is a signature of PDW order and that it is commensurately locked to the density wave stripes that are known to alternate orientation between adjacent layers. Even if the PDW is not the “mother of all state” [14–17], it is at least a close relative – possibly a second cousin.

Numerous studies have yielded highly suggestive but not yet universally convincing evidence that a novel form of superconducting order – PDW order – appears in some range of doping and temperature in certain high- $T_c$  cuprates [1–35]. The 2007 experimental observation in  $\text{La}_{1.875}\text{Ba}_{0.125}\text{CuO}_4$  (LBCO) by Li *et al.* [3] of “layer-decoupling” – i.e., superconductivity that appears to be confined to individual Cu-O layers accompanied by a spectacular absence of any detectable interlayer Josephson coupling – initiated an exciting area of study. Subsequent studies revealed similar transport phenomena in other La-based cuprates, including  $\text{La}_{2-x-y}\text{X}_y\text{Sr}_x\text{CuO}_4$  with  $X = \text{Nd}, \text{Eu}, \text{and Ca}$  [21–23], Fe and Zn-doped  $\text{La}_{2-x}\text{Sr}_x\text{CuO}_4$  (LSCO) [11, 12], and unadulterated LSCO with  $x = 0.1$  in the presence of a magnetic field [6], providing further support of the existence of a PDW state.

The 2019 observation in scanning tunneling microscopy (STM) by Edkins *et al* [9] of a PDW signature in another classic cuprate, Bi2212, represented a significant further breakthrough. They identified a subharmonic component of the CDW order in a halo region about magnetic field induced vortices, with ordering vector  $\vec{K}/2$  that is half of the ordering vector ( $\vec{K}$ ) of the primary CDW order [36]. Thus,  $\vec{K}/2$  is “subharmonic” order which, as we will discuss below, is of the sort expected whenever there is coexisting PDW order with  $\vec{Q} = \vec{K}/2$  and uniform SC. This same theory pertains, at least at mean-field level, to vortex cores under the assumption that in a state with dominant uniform superconducting order, a subdominant PDW order can emerge in the vortex core where the dominant order is suppressed [9, 15, 17, 34]. Moreover, similar patterns of CDW order are expected to arise in regimes where the PDW and/or the uniform superconducting order are fluctuating, assuming they have sufficiently long correlation lengths.

Nevertheless, several distinct aspects in Bi2212 compared with other cuprates pose challenges to fully understanding the broader implications of the PDW evidence. These aspects include the relatively short correlation length of CDW order, at best marginally longer than the CDW period [38–40] (hereafter, referred to as CDW short-range-order, CDW-SRO), the limited information concerning SDW order at zero magnetic field [41], and the lack of any macroscopic evidence (e.g., layer-decoupling) of PDW order. More generally, there have been no bulk (e.g., diffraction) measurements that show evidence of a subharmonic signature in La-based, Bi2212, YBCO, or indeed any cuprate, although various experiments [42–46] have been carried out in regimes where it would be expected were PDW order ubiquitous.

Here, we report the first bulk evidence of subharmonic order (i.e., a 1Q peak) in two

La-based near 1/8 doped cuprates, Sr-doped LBCO and Fe-doped LSCO. (For details see the Methods section.) We employed resonant soft x-ray scattering (RSXS) in conjunction with neutron scattering and transport measurements for a comprehensive study of the PDW state. We found that the long-sought 1Q peak appears as a new peak seen with RSXS for temperatures roughly midway between  $T_c$  and  $T_{\text{pdw}}$ , where  $T_{\text{pdw}}$  is, respectively, taken to be the  $T$  at which there is a sudden superconducting-like drop of the in-plane resistivity,  $\rho_{ab}$ , with no accompanying decrease in the interplane resistivity,  $\rho_c$  (i.e., there is still no SC-LRO). The new ordering vector  $\vec{K}/2$  is half that of the dominant CDW order. These results effectively address the challenges of PDW experiments (discussed below) and provide a foundation for further investigation into PDW and its implications in high- $T_c$  cuprates.

**Considerations of Intertwined orders:** Several well-known [31] aspects of PDW order and its relation to the other orders observed in the cuprates are worth reviewing before turning to the principle experimental findings. The relevant order parameters are the complex charge  $2e$  fields,  $\Delta_0$ ,  $\Delta_{\pm\vec{Q}}$ , and  $\Delta_{\pm\vec{Q}'}$ , that represent the local amplitude of the uniform and PDW components of the superconducting (SC) order, and the scalar and spin-vector fields,  $\rho_{\vec{K}}$ ,  $\rho_{\vec{K}'}$ ,  $\mathbf{S}_{K_{\text{sdw}}}$ , and  $\mathbf{S}_{K'_{\text{sdw}}}$  that represent the local amplitude of the CDW and SDW orders. Here the pairs of momenta  $[\vec{Q} \ \& \ \vec{Q}']$ ,  $[\vec{K} \ \& \ \vec{K}']$ , and  $[\vec{K}_{\text{sdw}} \ \& \ \vec{K}'_{\text{sdw}}]$  are related to each other by a  $C_4$  rotation of the crystal axes.

Each of these is, in principle, an independent order parameter with their own preferred ordering vector. In the present La-214 family of cuprates, the CDW and SDW orders are always commensurately locked to each other, i.e.,  $\vec{K} \equiv 2\vec{K}_{\text{sdw}}$  [11, 47–50], but this is not necessarily the case universally in the other cuprates [51]. There is compelling evidence that both SDW and CDW order strongly compete with uniform SC order. However, PDW order, when mutually commensurate with the other density wave orders (i.e., when  $\vec{K} \equiv 2\vec{Q}$ ), appears able to coexist with density wave order more easily – a point we revisit below.

As was known from previous studies, the phase diagrams of the La-cuprates studied here, including crossovers associated with the onset of density wave (DW) orders, have the same structure, shown schematically in Fig. 1, as that found for LBCO by Li *et al* [3]. There is an onset of CDW-SRO below a high-temperature crossover, a more sharply defined transition (or possibly two distinct transitions) at a stripe ordering temperature to a state with clear unidirectional CDW (below  $T_{\text{cdw}}$ ) and SDW “stripe” order (below  $T_{\text{sdw}} \leq T_{\text{cdw}}$ ) with long correlation lengths, a temperature at which layer-decoupling (i.e. a precipitous drop of  $\rho_{ab}$ )

develops at  $T_{\text{pdw}} \leq T_{\text{sdw}}$  (which we identify as the PDW transition temperature), and finally a transition at  $T_c$  to a 3D superconducting state in which  $\rho_c$  also vanishes and the perfect diamagnetism of the Meissner phase is apparent in measurements of the magnetization. The data showing this evolution in our crystal of Sr doped LBCO is shown in Fig. 3; comparable data for the Fe doped LSCO case were reported in the previous study [11].

**Theoretical considerations concerning a 1Q peak:** Because the evidence of PDW order has been somewhat hodge-podge, many discussions of cuprate physics do not include any reference to such order at all. Among the theoretical approaches that include it, there are two extremes in terms of perspective: (i) The “subdominant order” view, in which the uniform SC, CDW and SDW orders are the principle orders while PDW order appears - if at all - where the other orders are not too strong. (ii) The “mother of all orders” view [14–17, 55] which proposes that PDW ordering is the strongest, or one of the strongest ordering tendencies. This latter perspective underlies the suggestion that some form of fluctuating PDW order is much more robust than uniform SC order, such that it gives rise to the pseudo-gap phenomena at temperatures well above  $T_c$ , and to the suggestion that all observed CDW correlations arise as second harmonics of an underlying primary PDW order – i.e., they arise when and only when PDW correlations are strong.

To better frame the issue, let us consider the case in which all the density waves are assumed to be mutually commensurate, i.e.,  $\vec{K} \equiv 2\vec{Q} \equiv 2\vec{K}_{\text{sdw}}$ , and imagine that all the different order parameters can be considered as independent dynamical variables [56]. Then we expect the charge-density structure factor would have peaks at  $\vec{K}$  and  $\vec{K}/2 = \vec{Q}$  with intensities as follows:

$$\begin{aligned} I(\vec{K}) &\sim \left| \rho_{\vec{K}} + \alpha_{\text{sc}} \left[ \Delta_{-\vec{Q}}^* \Delta_{\vec{Q}} + c.c. \right] + \alpha_{\text{sdw}} \left[ \mathbf{S}_{-\vec{K}_{\text{sdw}}}^* \cdot \mathbf{S}_{\vec{K}_{\text{sdw}}} + c.c. \right] \right|^2, \\ I(\vec{Q}) &\sim |\alpha_{\text{sc}}|^2 \left| \Delta_0^* \Delta_{\vec{Q}} + c.c. \right|^2, \end{aligned} \quad (1)$$

where  $\alpha_{\text{sc}}$  and  $\alpha_{\text{sdw}}$  are coupling constants that depend on microscopic details. What is apparent here is that there could be multiple contributions to the scattering intensity at  $\vec{K}$ : It could primarily reflect CDW order if the fundamental CDW order is strong, or conversely if there were no intrinsic CDW ordering tendency, it could be an indirect signature of either PDW or SDW order. On the other hand, a  $1\vec{Q}$  peak clearly signifies an interference effect between the PDW and the uniform SC orders.

Motivated by the theoretical framework outlined above, we devised an experimental strat-

egy to identify a putative 1Q peak within our crystals (see details in the Method section). Specifically, we have chosen materials that exhibit layer-decoupling, indicative of the presence of significant PDW order, and have focused on two such materials that have relatively higher values of  $T_c$ 's, suggestive of a somewhat stronger tendency to develop uniform SC order. We have used the fact that there is little evidence of any density wave or SC order with significant correlation lengths at temperatures above  $T_{\text{cdw}}$  to identify high temperature scattering data as the uninteresting background signal (Extended data Fig. 1), which we can then subtract from the lower temperature data to obtain information about the interesting CDW correlations. Finally, we have chosen our scattering geometry to optimize the intensity of the 1Q peak. Together, these features have allowed us to extract clear evidence of a 1Q peak – a subharmonic of the dominant CDW order – that appears in the midst of the temperature range  $T_c < T < T_{\text{pdw}}$ , where it is theoretically expected.

**Experimental search for a 1Q signature in Fe-doped LSCO:** The first set of new results reported here (see Fig. 2) involve x-ray scattering from a previously studied crystal of Fe-doped LSCO [11] which exhibits bulk SC below  $T_c \approx 6$  K and layered-decoupling (2D-SC) below  $T_{\text{pdw}} = 32$  K (see detailed in the Method section). At  $T = 60$  K (see Fig. 2a), the RSXS map exhibits a weak signal indicative of CDW-SRO with a correlation length (21 Å) at  $h \approx 0.24$  r.l.u. (i.e.,  $\vec{K}$ ). As the temperature decreases to  $T = 43$  K (below  $T_{\text{sdw}} \approx 50$  K), the CDW signal becomes considerably stronger. Further cooling to  $T = 25$  K (situated below  $T_{\text{pdw}}$ ), results in a distinctly sharper CDW stripe ordering peak, characterized by a correlation length ( $\xi_{\vec{K}} \approx 61$  Å) that surpasses 8 unit cells ( $8a \approx 30$  Å) along the  $a$ -axis, in line with prior studies [11, 49]. In addition, at  $T = 25$  K, an excess of intensity distribution around  $\vec{K}/2$  is observed (indicated by the arrow in the figure). Figure 2b shows the intensity of  $h$ -scans integrated over the  $k$ -direction at each temperature. As the CDW signal grows with decreasing temperature, the intensity around the CDW peak's tail at  $h \sim 0.2$  r.l.u., marked as an arrow in the figure, increases. In addition, below  $T_{\text{pdw}}$ , a discernible background variation (indicated by the green-colored dashed line in the figure), also emerges, which is distinct from the contributions of the CDW tail and reflection intensities. Figure 2c further illustrates this variation with an extended  $h$  value scale. The excess intensity distribution emerges around  $\vec{K}/2$ , where the 1Q peak is expected.

Direct interpretation of the measured scattering intensity is complicated by the presence of a large background signal arising from fluorescence and specular reflection from the sample

surface (Extended Data Fig. 1). However, these are expected to be largely independent of temperature, so can be removed by subtracting the RSXS maps measured at two different temperatures, as shown in Figs. 3a and 3b. These subtractions provide direct information about the temperature dependent changes in the scattering intensities – A more detailed justification of this subtraction is described in the Method section. The results reveal a 1Q signature in this crystal that is weaker than, but coexists with the primary CDW stripe signal. Additional information concerning the  $T$  dependence of this structure can be gleaned by comparing the difference signal between a pair of temperatures just above and just below  $T_{\text{pdw}}$  (i.e., 25 K and 43 K) and two temperatures both above  $T_{\text{pdw}}$  (i.e., 43 K and 60 K), as depicted in Fig. 3c. We observe that a distinct ordering feature at  $h \approx 0.131 \pm 0.007$  r.l.u. ( $= \vec{K}/2 = \vec{Q}$ ) emerges below  $T_{\text{pdw}}$  (with a peak width corresponding to a correlation length,  $\xi_{\vec{Q}} \approx 43.47$  Å), while the feature at  $h \approx 0.235 \pm 0.005$  r.l.u. ( $= \vec{K} = 2\vec{Q}$ ) is clear both above and below  $T_{\text{pdw}}$ . Moreover, by examining the x-ray photon energy dependence (Fig. 3d and Extended Data Fig. 2), we found that the ordering features are associated with the Cu ions.

**1Q signature in other La-based cuprates:** To rule out the possibility that the (relatively weak) 1Q peak we have seen in Fe-doped LSCO is a peculiarity of one particular material, we conducted additional scattering experiments on another high- $T_c$  cuprate, Sr-doped LBCO. This choice was intentional as LBCO is the archetypal system in PDW research. Furthermore, based on the previous work [47, 48], the light Sr-doping leads to an enhancement of  $T_c$  and the suppression of the CDW compared to pristine LBCO; both features are expected to help in resolving signatures of subharmonic order.

In our initial assessment of this material’s suitability for our study, we examined DWs and superconducting properties to verify that the basic structure of the phase diagram is as in Fig. 1. Figures 4a and 4b show the CDW measured by RSXS and SDW measured by neutron scattering, respectively (see the Method). Similar to undoped LBCO, both DWs exhibit clear features as temperature decreases. The scattering data were analyzed and summarized in Figs. 4c and 4d. Consistent with the intertwined DW phenomena discussed earlier, the doped LBCO system undergoes a transition from CDW-SRO to a CDW stripe, accompanied by the emergence of SDW at  $T_{\text{sdw}} \approx 35.4$  K. At this temperature, the correlation length of the CDW stripe order ( $\xi_{\text{cdw}} \approx 90$  Å) already exceeds  $8a$  ( $\approx 30$  Å). The in-plane resistivity as shown in Fig. 4e confirms the emergence of significant 2D SC correlations, also below  $T \approx 35.4$  K (i.e.,  $T_{\text{pdw}} \approx T_{\text{sdw}}$ ), which is distinctly different

from the bulk superconducting transition temperature ( $T_c \approx 10$  K) determined by magnetic susceptibility. In addition, the relatively suppressed strength of the overall CDW order in the Sr-doped LBCO relative to the pristine material, as well as the correspondingly weak background, which are consistent with findings of previous studies [47, 48], are helpful for detecting subharmonic order below  $T_{\text{pdw}}$ .

Figure 5a presents the RSXS maps obtained from Sr-doped LBCO; with additional experimental details reported in the Method section. At  $T = 42.5$  K (upper panel in Fig. 5a), where the stripe phase has not yet developed, the scattering map shows the CDW-SRO signal. Consistent with the discussion in Fig. 4, the RSXS map measured at 26.5 K (i.e., below  $T_{\text{pdw}}$ ) exhibits pronounced CDW intensity at  $h \approx 0.235 \pm 0.005$  r.l.u., indicating the development of the stripe phase. Furthermore, there appears to be enhanced intensity at  $h \approx 0.12 \pm 0.007$  r.l.u.

Adopting the same method of analysis we used for Fe-doped LSCO, we exhibit the difference between the RSXS maps measured at  $T = 26.5$  K and 42.5 K in Fig. 5b. The subtracted (i.e., difference) map reveals intensity in the expected regions. Not only is the CDW stripe clearly evident, but a notable emergence of 1Q order is also apparent below  $T_{\text{pdw}}$ . These results bear a striking resemblance to the observations made in the context of the Fe-doped LSCO cuprate, confirming the robustness of the findings.

Figures 5c and 5d show the projected intensities derived from the difference map along various cuts through reciprocal space. Recalling that  $\vec{K} \approx (h = 1/4, k = 0)$  and  $\vec{Q} = \vec{K}/2 \approx (h = 1/8, k = 0)$ , in Fig. 5c we display the scattering intensity along the  $k$  direction integrated over  $0.10 < h < 0.15$  r.l.u. and  $0.21 < h < 0.26$  r.l.u. (shown as the green circles and the solid blue line, respectively). In common with what is seen at low doping in LSCO [49, 57, 58], the CDW peak in Sr-doped LBCO is relatively broad in this direction with a slight two-peak structure along the  $k$ -direction at  $h \approx 1/4$ . This feature reflects the coexistence of the LTO and LTT structural phases [47, 48]. As anticipated in Eq.(1), a comparable splitting effect is discernible in the subharmonic order along the corresponding cut through  $k$ -space. In Fig. 5d, we show data taken at different detector-angles ( $2\theta$ ). A subtlety of the way the experiments are carried out is that all cuts through  $q$ -space traverse a trajectory that has a fixed  $2\theta$  relative to the  $ab$ -plane as shown in the extended data Fig. 3. This means there is an implicit  $l$  dependence of the data. All the density wave orders seen in these materials are quasi-2D, which is to say that the  $l$  dependence is relatively



smooth, but none-the-less, the primary CDW order has been long known to have maximal intensity at half-integer  $l$  (Extended data Fig. 3a). For  $2\theta = 123^\circ$ , the  $q$ -space trajectory passes through the principle stripe-ordering vector  $\vec{K}$  at  $l \approx 1.5$  r.l.u., while at the position of the 1Q peak,  $l \approx 1.3$  r.l.u. Conversely, the trajectory with  $2\theta = 106^\circ$  passes through the stripe ordering vector at  $l \approx 1.7$  r.l.u., and through the 1Q peak at  $l \approx 1.5$  r.l.u. Both cuts show the principle stripe-ordering peak clearly, albeit the first cut shows it more clearly. But because it is weak, it is only in the second cut where conditions are optimized that the 1Q peak is evident. In addition to providing information pertinent to avoiding a possible failure route in future studies of this order, this observations demonstrates that the 1Q peak shares the same interlayer structure as the principle stripe-order peak.

**Discussion:** In this work, we have observed subharmonic (1Q) CDW order with a structure that links it with the fundamental quasi-2D CDW order. The fundamental (2Q) is always much stronger, and is seen over a wide range of  $T$ , while the subharmonic is only observable below  $T_{\text{pdw}}$ , where observed layer-decoupling phenomena already provided strong indirect evidence of the existence of PDW order. Together, these results provide compelling evidence of the theoretically conjectured state consisting of mutually commensurate CDW, SDW, and PDW orders.

An intuitive real-space image for such a state can be visualized starting with the familiar “stripe” image (suggestive Extended data Fig. 3b) [25] of regions of Néel antiferromagnetic order separated by a periodic array of anti-phase boundaries at which the density of itinerant (doped) holes is maximal. The PDW order would then be expected to be shifted by half a period relative to the SDW order, such that the pair-field has maximum magnitude where the itinerant hole density is largest, and vanishes where the pair-field changes sign in the midst of the spin-ordered regions. This complex state, while theoretically conjectured, remains challenging to directly visualize. Nevertheless, a state with PDW order but no long-range uniform SC order is distinct by symmetry from any usual SC state, including states with coexisting CDW and SDW order. It is a distinct phase of matter. Thus, establishing its existence is significant, independent of any broader importance of this result for the physics of the high- $T_c$  cuprates.

Turning to the cuprates, the present results extend the evidence that a central feature of the physics [31] is the existence of a large number of distinct forms of order all of which onset in the same range of temperatures (roughly from 30K - 150K), and which are strongly

“intertwined” in the sense that they are strongly coupled to each other but neither inevitably coexist nor universally compete with one another. Manifestly, PDW order can now be added to the list of established intertwined orders – *d*-wave SC, CDW, SDW, and possibly nematic.

Somewhat more speculatively, the present results support the conclusion that PDW order is typically subdominant relative to competing uniform SC order, and occurs only where the dominant order is in some way significantly weakened. For instance, investigations into a 1Q peak in YBCO have been carried out over a range of magnetic fields and strain where global SC order coexists with pronounced signals of charge-density wave (CDW) order (at  $\vec{K} = 2\vec{Q}$ ). If CDW order were primarily a harmonic of PDW order, a prominent 1Q peak would have been anticipated alongside the CDW signal [42, 43]. However, in contrast to the outcomes observed in La-based cuprates here, the emergence of a 1Q peak has not been reported. Based on the considerations discussed, our assessment suggests that the perspective of a “mother of all orders,” while intriguing, lacks consistency with a variety of observations in cuprates. Indeed, the subdominant PDW order perspective offers a plausible explanation for the elusiveness of the 1Q peak; to see it one has to identify circumstances in which the uniform SC component, which typically prevents PDW order, is relatively weak but not entirely eliminated. Importantly, although CDW and SDW order likely also compete with PDW order [59], the real-space picture presented above makes it plausible that this competition is much less strong for PDW than for uniform SC order. In the sense that “the enemy of my enemy is my friend,” one can anticipate that relatively strong CDW and/or SDW order may effectively enhance PDW tendencies by suppressing the more strongly competitive uniform SC order.

Finally, it is worth highlighting the future experimental opportunities that arise from our current findings. Since our present experimental results lack phase-sensitive information, they do not directly corroborate certain aspects of the “stripe” image or conclusively address questions like whether the intertwined order is commensurate (i.e., precisely period 8), and if so, whether it is “site-centered” or “bond-centered.” Therefore, further investigations that explore the polarization and azimuthal dependence of this 1Q peak are warranted. In addition, conducting experiments in the presence of an external magnetic field holds the promise of yielding valuable insights into the characteristic behavior of the observed peak and its correlation with the 2D and 3D superconducting states. Furthermore, expanding the scope of x-ray measurements to encompass other cuprate materials, based on the criteria

established in this study, would offer an enriching avenue for research. These efforts will undoubtedly contribute to a deeper understanding of the complex interplay between various orders in the high- $T_c$  cuprates.

## METHODS

**Synthesis of single crystals:** High-quality single crystals of both Sr-doped LBCO ( $\text{La}_{2-1/8}\text{Ba}_{1/8-0.06}\text{Sr}_{0.06}\text{CuO}_4$ ) and Fe-doped LSCO ( $\text{La}_{1.87}\text{Sr}_{0.13}\text{Cu}_{0.99}\text{Fe}_{0.01}\text{O}_4$ ) were grown by the traveling solvent floating zone method. The grown crystal was annealed in one bar of  $\text{O}_2$  gas to minimize oxygen deficiencies. The typical growth rate was 1.0 mm/hr and a 50–60 mm long crystal rod was successfully obtained for each concentration. Before the scattering measurements, using a Quantum Design PPMS we characterized their superconducting  $T_c$  as the mid-point of the transition. To check the crystal properties, the in-plane electrical resistivity and magnetic susceptibility measurements of the crystal was measured by the conventional four-point probe method at the Institute for Materials Research, Tohoku University. For elastic neutron scattering measurements, a crystal of Sr-doped LBCO (Fe-doped LSCO) with the length of 25mm (35mm) was used. For the RSXS measurements, we prepared all the samples with a typical dimension of 1.5 mm  $\times$  1.5 mm  $\times$  2.5 mm ( $a \times b \times c$  axis). To achieve a fresh  $c$ -axis normal surface, each sample was ex-situ cleaved, before transported into the ultra-high vacuum chamber (base pressure =  $8 \times 10^{-10}$  Torr).

**RSXS measurement:** The zero-magnetic field x-ray experiments were conducted at beamline 13-3 of the Stanford Synchrotron Radiation Lightsource (SSRL). The sample was positioned on an in-vacuum 4-circle diffractometer and maintained at a controlled temperature using an open-circle helium cryostat (base  $T \approx 25$  K). To avoid distortions of the cryostat and mechanical components of the diffractometer typically occurred during initial cool down or large temperature changes, we ensured that the setup had sufficient time to stabilize at each measurement temperature and the temperature did not exceed 100K during the whole data collection. Incident photon polarization was consistently set as vertical linear ( $\sigma$ ) polarization. The precise ( $h, 0, l$ ) scattering plane alignment was achieved using the measured (0, 0, 2), (-1, 0, 1), and (1, 0, 1) structural Bragg reflections at a photon energy of approximately 1770 eV.

Detecting the RSXS signals used a  $256 \times 1024$  pixel area detector. To ensure the maximized scattering intensity, we set the detector at a fixed position of  $2\theta = 106^\circ$  in which the scattering from  $\vec{Q}$  is at  $l \approx 1.5$ . We rotated the sample in small steps ( $\theta$ -scan) to gather information about the  $h$ -dependence. Throughout the  $\theta$ -scan, each CCD image included

scattering information from the well-aligned  $(h, 0, l)$  scattering plane near the center of the detector and from off-scattering planes  $(h, \pm k, l)$  at the top and bottom parts of the CCD [49]. For data analysis, each CCD pixel was translated into an  $hkl$  reciprocal space index. The resulting three-dimensional scattering intensity data were then projected onto different planes/directions for further analysis.

It is worth noting that the single scattering data collection at each temperature point involved a total of 8 hours of measurements. Due to the critical role of background information in shaping our data analysis strategy, meticulous signal-to-noise ratio reduction and x-ray footprint control were paramount considerations (see the section below - Strategy for detecting a 1Q peak).

Furthermore, it is important that the incident polarization for the experiment was chosen to be vertical because using linear polarization parallel to the scattering plane poses additional challenges. Specifically, when the 1Q's  $l$ -vector is around half-integer  $l$ , the  $2\theta$  angle approaches Brewster's angle. In other words, the charge scattering signal (i.e.,  $\pi' \cdot \pi$ ) is reduced by approximately  $1 - \cos(2\theta)$  without considering details of the scattering tensors' matrix elements based on the Cu orbital state in the  $\text{CuO}_2$  plane. In this scenario, the expected 1Q signal in  $\pi$ -polarization could be even less, approximately 70% lower than that in  $\sigma$ -polarization. Although other backgrounds, such as specular and CDW tails, would also be reduced, but it becomes more challenging when attempting to detect an intrinsically smaller 1Q signal in this type of experiment.

**Neutron measurement:** In order to investigate the SDW order, we performed the elastic neutron scattering measurements on the cold triple-axis spectrometer HER and the thermal neutron triple-axis spectrometer TOPAN located at the research reactor JRR-3. The most of measurements were performed at HER with the incident and scattered neutron energies of 5 meV. Additional elastic scattering measurements were carried out using the thermal neutron triple-axis spectrometer TOPAN at JRR-3. The horizontal collimations sequences at HER and TOPAN were 32'-100'-Be-S-80'-80 and 30'-Sap-30'-PG-S-PG-30'-100', respectively. Here Be, Sap and PG represent the beryllium, sapphire and pyrolytic graphite filters, respectively, to reduce contamination from the higher-order wavelength neutron in the beam. S denotes the sample. The single crystal was sealed in an aluminum can with Helium gas for thermal exchange. The aluminum can was attached to the closed-cycle cryostat to control

the temperature.

**Strategy for detecting a 1Q peak:** To optimize conditions for observing a 1Q peak, we begin by focusing on members of the 214 family in which clear signatures of layer-decoupling provide strongly suggestive evidence of significant PDW order. In the poster-child material for layer-decoupling, 1/8 doped LBCO, the CDW and SDW order are particularly strong, while  $T_c$  is 4 K or less, suggestive that the uniform SC order is all but absent in the range of temperatures that are accessible to us in RSXS. We therefore have looked at two closely related materials – Fe-doped LSCO and partially Sr substituted LBCO – both of which show a clear range of  $T$  in which layer-decoupling is apparent, but which have relatively higher values of  $T_c$  and somewhat weaker scattering at  $\vec{K}$ .

In resonant x-ray scattering, there are three purely technical challenges to observing a weak 1Q peak. The first is that the strength of the scattering off the principle CDW order implies technical challenges in observing a putative 1Q peak on the background coming from the tail of the  $\vec{K}$  peak (hereafter, CDW-tail). Given that this tail signal typically persists even at significantly off- $q$  positions (e.g.,  $\vec{Q}$ ), it would also be advantageous if the material exhibits a somewhat weaker scattering signal at  $\vec{K}$ , as discussed above. This further supports the rationale for our choice of these cuprates from a scattering perspective.

The second is that there is always a strong elastic background that has nothing to do with the desired diffraction signal that comes from a combination of specular scattering from the sample surface (i.e., reflection and its tail), and florescence (including the geometrical effect of a detector position). Fortunately, these two background sources are expected to be approximately temperature independent. Thus, we can remove it by subtracting the signal taken at relatively high temperatures,  $T = 60$  K (Fe-LSCO case), from the lower temperature signals as shown in Figs. 2 and 5. Since this is well above  $T_{\text{strp}} \approx 40$  K, we do not expect any significant CDW component to the high  $T$  signal, so this subtraction should be reasonably reliable.

The last arises from the expected dependence of the scattering intensity on the  $c$ -axis component of the scattering vector,  $l$ . It is known that the CDW scattering produces quasi-2D rods of scattering, so that one generally treats  $\vec{K}$  as a 2D vector. In this context, the CDW intensity is greatest at  $l = 1/2$  in reciprocal lattice units (r.l.u.), where is a doubled  $c$ -axis unit cell corresponding to a 4-Cu-O plane period. Assuming that the same is true of

the PDW order, then it would be expected that the 1Q scattering intensity would also be strongest at half-integer  $l$ . However, as shown in the extended data Fig. 1b, RSXS data is measured by rotating the sample at the fixed the detector in the scattering plane, meaning that as the scattering vector,  $q = (h, k, l)$ , traverses a given trajectory in the  $ab$  plane (for instance, variable  $h$  for fixed  $k$ ), the value of  $l$  is an implicit function of the position along this trajectory. Thus, it is customary to choose a trajectory such that  $l$  is half integer when the in-plane component of  $q$  equals  $\vec{K}$ . However, in this case, the value of  $l$  is typically far from a half-integer value when the in-plane component of  $q$  equals  $\vec{Q}$ . If, on the other hand, the trajectory is chosen so that  $l$  is half-integer for the in-plane component of  $q$  equal to  $\vec{Q}$ , one would expect enhanced 1Q scattering intensity, and reduced intensity at  $\vec{K}$  (see the extended data Fig. 3a). That this expectation is realized can be seen by comparing the results along two such trajectories in the following experimental results shown in Figs. 2 and 5.

Finally, to properly implement the aforementioned strategy, it is imperative to maintain high-quality data throughout prolonged acquisition times. The following steps were taken to ensure that the scattering signal was consistently originated from the same spot on the sample. First, two optical cameras continuously tracked both the x-ray beam and sample positions with micron-level resolution. Second, before and after each angle scan, we verified the positions of structural Bragg reflections  $(0, 0, 2)$ ,  $(-1, 0, 1)$ , and  $(1, 0, 1)$ . This ensured that the X-rays consistently probed the same domain structure and sample volume. Third, during the acquisition of photon signals (i.e., angular scan), we simultaneously recorded the secondary electron signal, known as total electron yield (TEY). The intensity of TEY is highly sensitive to incident x-ray beam angle with respect to the sample and beam footprint on the sample. We utilized the angular dependence of the TEY signal as a real-time indicator to ensure reproducibility.

---

\* jslee@slac.stanford.edu

- [1] Tajima, S. Noda, T. Eisaki, H. & Uchida, S. *c*-Axis Optical Response in the Static Stripe Ordered Phase of the Cuprates. *Phys. Rev. Lett.* **86**, 500 (2001).
- [2] Yuli, O. Asulin, I. Millo, O. & Koren, G. Scanning tunneling spectroscopy characterization of the pseudogap and the  $x=1/8$  anomaly in  $\text{La}_{2-x}\text{Sr}_x\text{CuO}_4$  thin films. *Phys. Rev. B* **75**, 184521 (2007).
- [3] Li, Q. Hücker, M. Gu, G. D. Tselik, A. M. & Tranquada, J. M. Two-Dimensional Superconducting Fluctuations in Stripe-Ordered  $\text{La}_{1.875}\text{Ba}_{0.125}\text{CuO}_4$ . *Phys. Rev. Lett.* **99**, 067001 (2007).
- [4] Yang, K. Y. Chen, W. Q. Rice, T. M. Sigrist, M. & Zhang, F. C. Nature of stripes in the generalized t-J model applied to the cuprate superconductors. *New J. Phys.* **11**, 055053 (2009).
- [5] Yuli, O. Asulin, I. Koren, G. & Millo, O. Spatial modulation of midgap states in (001)  $\text{La}_{1.88}\text{Sr}_{0.12}\text{CuO}_4$  films: Indications for antiphase ordering of the d-wave order parameter. *Phys. Rev. B* **81**, 024516 (2010).
- [6] Schafgans, A. A. LaForge, A. D. Dordevic, S. V. Qazilbash, M. M. Padilla, W. J. Burch, K. S. Li, Z. Q. Komiyama, S. Ando, Y. & Basov, D. N. Towards a Two-Dimensional Superconducting State of  $\text{La}_{2-x}\text{Sr}_x\text{CuO}_4$  in a Moderate External Magnetic Field. *Phys. Rev. Lett.* **104**, 157002 (2010).
- [7] Stegen, Z. Han, S. J. Wu, J. Pramanik, A. K. Hücker, M. Gu, G. Li, Q. Park, J. H. Boebinger, G. S. & Tranquada, J. M. Evolution of superconducting correlations within magnetic-field-decoupled  $\text{La}_{2-x}\text{Ba}_x\text{CuO}_4$  ( $x = 0.095$ ). *Phys. Rev. B* **87**, 064509 (2013).
- [8] Hamidian, M. H. Edkins, S. D. Joo, S. H. Kostin, A. Eisaki, H. Uchida, S. Lawler, M. J. Kim, E.-A. Mackenzie, A. P. Fujita, K. Lee, J. & Séamus Davis, J. C. Detection of a Cooper-pair density wave in  $\text{Bi}_2\text{Sr}_2\text{CaCu}_2\text{O}_{8+x}$ . *Nature* **532**, 343-347 (2016).
- [9] Edkins, S. D. Kostin, A. Fujita, K. Mackenzie, A. P. Eisaki, H. Uchida, S. Sachdev, S. Lawler, M. J. Kim, E.-A. Séamus Davis, J. C. & Hamidian, M. H. Magnetic field-induced pair density wave state in the cuprate vortex halo. *Science* **364**, 976-980 (2019).
- [10] Du, Z. Li, H. Joo, S. H. Donoway, E. P. Lee, J. Séamus Davis, J. C. Gu, G. Johnson, P. D. & Fujita, K. Imaging the energy gap modulations of the cuprate pair-density-wave state. *Nature*



- 580**, 65-70 (2020).
- [11] Huang, H. Lee, S.-J. Ikeda, Y. Taniguchi, T. Takahama, M. Kao, C.-C. Fujita, M. & Lee J.-S. Two-Dimensional Superconducting Fluctuations Associated with Charge-Density-Wave Stripes in  $\text{La}_{1.87}\text{Sr}_{0.13}\text{Fe}_{0.01}\text{CuO}_4$ . *Phys. Rev. Lett.* **126**, 167001 (2021).
- [12] Lozano, P. M. Gu, G. D. Tranquada, J. M. & Li, Q. Experimental evidence that zinc impurities pin pair-density-wave order in  $\text{La}_{2-x}\text{Ba}_x\text{CuO}_4$ . *Phys. Rev. B* **103**, L020502 (2021).
- [13] Lozano, P. M. Ren, T. Gu, G. D. Tsvelik, A. M. Tranquada, J. M. & Li, Q. Testing for pair density wave order in  $\text{La}_{1.875}\text{Ba}_{0.125}\text{CuO}_4$ . *Phys. Rev. B* **106**, 17451 (2022).
- [14] Lee, P. A. Amperean Pairing and the Pseudogap Phase of Cuprate Superconductors. *Phys. Rev. X* **4**, 031017 (2014).
- [15] Dai, Z. Zhang, Y.-H. Senthil, T. & Lee, P. A. Pair-density waves, charge-density waves, and vortices in high- $T_c$  cuprates. *Phys. Rev. B* **97**, 174511 (2018).
- [16] Lee, P. A. Proposal to measure the pair field correlator of a fluctuating pair density wave *Phys. Rev. B* **99**, 035132 (2019).
- [17] Agterberg, D. F. Séamus Davis, J. C. Edkins, S. D. Fradkin, E. Van Harlingen, D. J. Kivelson, S. A. Lee, P. A. Radzihovsky, L. Tranquada, J. M. & Wang, Y. The Physics of Pair-Density Waves: Cuprate Superconductors and Beyond. *Annu. Rev. Condens. Matter Phys.* **11**, 231-270 (2020).
- [18] Zelli, M. Kallin, C. & Berlinsky, A. J. Quantum oscillations in a  $\pi$ -striped superconductor. *Phys. Rev. B* **86**, 104507 (2012).
- [19] Yu, F. Hirschberger, M. Loew, T. Li, G. Lawson, B. J. Asaba, T. Kemper, J. Liang, T. Porras, J. Boebinger, G. S. Singleton, J. Keimer, B. Li, L. & Ong, N. P. Magnetic phase diagram of underdoped  $\text{YBa}_2\text{Cu}_3\text{O}_y$  inferred from torque magnetization and thermal conductivity. *Proc. Natl. Acad. Sci. U.S.A.* **113**, 12667 (2016).
- [20] Norman M. R. & Séamus Davis, J. C. Quantum oscillations in a biaxial pair density wave state. *Proc. Natl. Acad. Sci. U.S.A.* **115**, 5389 (2018).
- [21] Ding, J. F. Xiang, X. Q. Zhang, Y. Q. Liu, H. & Li, X. G. Two-dimensional superconductivity in stripe-ordered  $\text{La}_{1.6-x}\text{Nd}_{0.4}\text{Sr}_x\text{CuO}_4$  single crystals. *Phys. Rev. B* **77**, 214524 (2008).
- [22] Shi, Z., Baity, P.G., Terzic, J. Sasagawa, T. & Popović, D. Pair density wave at high magnetic fields in cuprates with charge and spin orders. *Nat. Commun.* **11**, 3323 (2020).
- [23] Zhong, R. Schneeloch, J. A. Chi, H. Li, Q. Gu, G. & Tranquada, J. M. Evidence for magnetic-

- field-induced decoupling of superconducting bilayers in  $\text{La}_{2-x}\text{Ca}_{1+x}\text{Cu}_2\text{O}_6$ , *Phys. Rev. B* **97**, 134520 (2018).
- [24] Himeda, A. Kato, T. & Ogata, M. Stripe States with Spatially Oscillating d-Wave Superconductivity in the Two-Dimensional  $t - t' - J$  Model. *Phys. Rev. Lett.* **88**, 117001 (2002).
- [25] Berg, E. Fradkin, E. Kim, E.-A. Kivelson, S. A. Oganessian, V. Tranquada, J. M. & Zhang, S. C. Dynamical Layer Decoupling in a Stripe-Ordered High- $T_c$  Superconductor. *Phys. Rev. Lett.* **99**, 127003 (2007).
- [26] Berg, E. Fradkin, E. Kivelson, S. A. & Tranquada, J. M. Striped superconductors: how spin, charge and superconducting orders intertwine in the cuprates. *New J. Phys.* **11**, 115004 (2009).
- [27] Berg, E. Fradkin, E. & Kivelson, S. A. Charge- $4e$  superconductivity from pair-density-wave order in certain high-temperature superconductors. *Nature Physics* **5**, 830-833 (2009).
- [28] Radzihovsky, L & Vishwanath, A. Quantum Liquid Crystals in an Imbalanced Fermi Gas: Fluctuations and Fractional Vortices in Larkin-Ovchinnikov States. *Phys. Rev. Lett.* **103**, 010404 (2009).
- [29] Yang, K. Y. Chen, W. Q. Rice, T. M. Sigrist, M. & Zhang, F. C. Nature of stripes in the generalized t-J model applied to the cuprate superconductors. *New J. Phys.* **11**, 055053 (2009).
- [30] Agterberg, D. F. & Tsunetsugu, H. Dislocations and vortices in pair-density-wave superconductors. *Nature. Phys.* **4**, 639-642 (2008).
- [31] Fradkin, E. Kivelson, S. A. & Tranquada, J. M. Colloquium: Theory of intertwined orders in high temperature superconductors. *Rev. Mod. Phys.* **87**, 457 (2015).
- [32] Mross, D. F. & Senthil, T. Spin- and Pair-Density-Wave Glasses. *Phys. Rev. X* **5**, 031008 (2015).
- [33] Cai, R.-G. Li, L. Wang, Y.-Q. & Zaanen, J. Intertwined Order and Holography: The Case of Parity Breaking Pair Density Waves. *Phys. Rev. Lett.* **119**, 181601 (2017).
- [34] Wang, Y. Edkins, S. D. Hamidian, M. H. Séamus Davis, J. C. Fradkin, E. & Kivelson, S. A. Pair density waves in superconducting vortex halos. *Phys. Rev. B* **97**, 174510 (2018).
- [35] Agterberg, D. F. & Garaud, J. Checkerboard order in vortex cores from pair-density-wave superconductivity. *Phys. Rev. B* **91**, 104512 (2015).
- [36] A slightly later STM study [10] reported evidence, also in Bi2212 but without any magnetic field, of a small PDW component on a background of a stronger uniform superconductivity, but neither the theory of this effect nor the experimental evidence is as clear as for the vortex

cores.

- [37] Berg, E., Fradkin, E., and Kivelson, S. A., Theory of the striped superconductor. *Phys. Rev. B* **79**, 064515 (2009).
- [38] da Silva Neto, E. H. Aynajian, P. Frano, A. Comin, R. Schierle, E. Weschke, E. Gyenis, A. Wen, J. Schneeloch, J. Xu, Z. Ono, S. Gu, G. Le Tacon, M. & Yazdani, A. Ubiquitous Interplay Between Charge Ordering and High-Temperature Superconductivity in Cuprates. *Science* **343**, 393 (2014).
- [39] Lu, H. Hashimoto, M. Chen, S.-D. Ishida, S. Song, S. Eisaki, H. Nag, A. Garcia-Fernandez, M. Arpaia, R. Ghiringhelli, G. Braicovich, L. Zaanen, J. Moritz, B. Kummer, K. Brookes, N. B. Zhou, K.-J. Shen, Z.-X. Devereaux, T. P. & Lee, W.-S. Identification of a characteristic doping for charge order phenomena in Bi-2212 cuprates via RIXS. *Phys. Rev. B* **106**, 155109 (2022).
- [40] Chaix, L. Ghiringhelli, G. Peng, Y. Y. Hashimoto, M. Moritz, B. Kummer, K. Brookes, N. B. He, Y. Chen, S. Ishida, S. Yoshida, Y. Eisaki, H. Salluzzo, M. Braicovich, L. Shen, Z.-X. Devereaux, T. P. & Lee, W.-S. Dispersive charge density wave excitations in  $\text{Bi}_2\text{Sr}_2\text{CaCu}_2\text{O}_{8+\delta}$ . *Nature Phys.* **13**, 952-956 (2017).
- [41] Mounce, A. M. Oh, S. Mukhopadhyay, S. Halperin, W. P. Reyes, A. P. Kuhns, P. L. Fujita, K. Ishikado, M. & Uchida, S. Spin-Density Wave near the Vortex Cores in the High-Temperature Superconductor  $\text{Bi}_2\text{Sr}_2\text{CaCu}_2\text{O}_{8+y}$ . *Phys. Rev. Lett.* **106**, 057003 (2011).
- [42] Vinograd, I. Souliou, S. M. Haghighirad, A.-A. Lacmann, T. Frachet, M. Merz, M. Maraytta, N. Garbarino, G. Liu, Y. Nakata, S. Ishida, K. Noad, H. M. L. Minola, M. Keimer, B. Hicks, C. W. & Le Tacon, M. Strain-Tuning of 2D and 3D Charge-Density Waves in High-Temperature Superconducting  $\text{YBa}_2\text{Cu}_3\text{O}_y$ . <https://doi.org/10.48550/arXiv.2308.08395> (2023).
- [43] Blackburn, E. Ivashko, O. Campillo, E. Zimmermann, M. v. Liang, R. Bonn, D. A. Hardy, W. N. Chang, J. Forgan, E. M. & Hayden, S. M. Searching for the signature of a pair density wave in  $\text{YBa}_2\text{Cu}_3\text{O}_{6.67}$  using high energy X-ray diffraction. <https://doi.org/10.48550/arXiv.2310.18302> (2023).
- [44] Peng, Y. Y. Salluzzo, M. Sun, X. Ponti, A. Betto, D. Ferretti, A. M. Fumagalli, F. Kummer, K. Le Tacon, M. Zhou, X. J. Brookes, N. B. Braicovich, L. & Ghiringhelli G. Direct observation of charge order in underdoped and optimally doped  $\text{Bi}_2(\text{Sr},\text{La})_2\text{CuO}_{6+\delta}$  by resonant inelastic x-ray scattering. *Phys. Rev. B* **94**, 184511 (2016).

- [45] Chaix, L Ghiringhelli, G. Peng, Y. Y. Hashimoto, M. Moritz, B. Kummer, K. Brookes, N. B. He, Y. Chen, S. Ishida, S. Yoshida, Y. Eisaki, H. Salluzzo, M. Braicovich, L. Shen, Z.-X. Devereaux T. P. & Lee, W.-S. Dispersive charge density wave excitations in  $\text{Bi}_2\text{Sr}_2\text{CaCu}_2\text{O}_{8+\delta}$ . *Nature Phys.* **13**, 952 (2017).
- [46] Schafgans, A. A. LaForge, A. D. Dordevic, S. V. Qazilbash, M. M. Padilla, W. J. Burch, K. S. Li, Z. Q. Komiya, S. Ando, Y. & Basov, D. N. Towards a Two-Dimensional Superconducting State of  $\text{La}_{2-x}\text{Sr}_x\text{CuO}_4$  in a Moderate External Magnetic Field. *Phys. Rev. Lett.* **104**, 157002 (2010).
- [47] Fujita, M, Goka, H. Yamada, K. Tranquada, J. M. & Regnault, L. P. Stripe order, depinning, and fluctuations in  $\text{La}_{1.875}\text{Ba}_{0.125}\text{CuO}_4$  and  $\text{La}_{1.875}\text{Ba}_{0.075}\text{Sr}_{0.050}\text{CuO}_4$ . *Phys. Rev. B* **70**, 104517 (2004).
- [48] Fujita, M. Goka, H. Yamada, K. & Matsuda, M. Competition between Charge- and Spin-Density-Wave Order and Superconductivity in  $\text{La}_{1.875}\text{Ba}_{0.1252-x}\text{Sr}_x\text{CuO}_4$ . *Phys. Rev. Lett.* **88**, 167008 (2002).
- [49] Wen, J.-J. Huang, H. Lee, S.-J. Jang, H. Knight, J. Lee, Y. S. Fujita, M. Suzuki, K. M. Asano, S. Kivelson, S. A. Kao, C.-C. & Lee, J.-S. Observation of two types of charge-density-wave orders in superconducting  $\text{La}_{2-x}\text{Sr}_x\text{CuO}_4$ . *Nat. Commun.* **10**, 3269 (2019).
- [50] Yamada, K. Lee, C. H. Kurahashi, K. Wada, J. Wakimoto, S. Ueki, S. Kimura, H. Endoh, Y. Hosoya, S. Shirane, G. Birgeneau, R. J. Greven, M. Kastner, M. A. & Kim, Y. J. Doping dependence of the spatially modulated dynamical spin correlations and the superconducting-transition temperature in  $\text{La}_{2-x}\text{Sr}_x\text{CuO}_4$ . *Phys. Rev. B* **57**, 6165-6172 (1998).
- [51] When CDW and SDW order are mutually commensurate, each order enhances the other as is the case in the present materials, while when they are mutually incommensurate, they tend to compete as in YBCO [53, 54].
- [52] Arpaia, R. Caprara, S. Fumagalli, R. De Vecchi, G. Peng, Y. Y. Andersson, E. Betto, D. De Luca, G. M. Brookes, N. B. Lombardi, F. Salluzzo, M. Braicovich, L. Di Castro, C. Grilli, M. & Ghiringhelli, G. Dynamical charge density fluctuations pervading the phase diagram of a Cu-based high-Tc superconductor. *Science* **365**, 906–910 (2019).
- [53] Blanco-Canosa, S. Frano, A. Schierle, E. Porras, J. Loew, T. Minola, M. Bluschke, M. Weschke, E. Keimer, B. & Le Tacon M. Resonant x-ray scattering study of charge-density wave correlations in  $\text{YBa}_2\text{Cu}_3\text{O}_{6+x}$ . *Phys. Rev. B* **90**, 054513 (2014).

- [54] Haug, D. Hinkov, V. Sidis, Y. Bourges, P. Christensen, N. B. Ivanov, A. Keller, T. Lin, C. T. & Keimer, B. Neutron scattering study of the magnetic phase diagram of underdoped  $\text{YBa}_2\text{Cu}_3\text{O}_{6+x}$ . *New J. Phys.* **12**, 105006 (2010).
- [55] Wang, S. Choubey, P. Chong, Y. X. Chen, W. Ren, W. Eisaki, H. Uchida, S. Hirschfeld, P. J. & Séamus Davis, J. C. Scattering interference signature of a pair density wave state in the cuprate pseudogap phase. *Nat. Commun.* **12**, 6087 (2021).
- [56] Although  $2\vec{Q} \equiv 2\vec{K}_{\text{sdw}}$ , we expect that  $\vec{K}_{\text{sdw}} - \vec{Q} = (1/2, 1/2)$ .
- [57] Thampy, V. Dean, M. P. M. Christensen, N. B. Steinke, L. Islam, Z. Oda, M. Ido, M. Momono, N. Wilkins, S. B. & Hill, J. P. Rotated stripe order and its competition with superconductivity in  $\text{La}_{1.88}\text{Sr}_{0.12}\text{CuO}_4$ . *Phys. Rev. B* **90**, 100510 (2014).
- [58] Kimura, H. Matsushita, H. Hirota, K. Endoh, Y. Yamada, K. Shirane, G. Lee, Y. S. Kastner, M. A. & Birgeneau, R. J. Incommensurate geometry of the elastic magnetic peaks in superconducting  $\text{La}_{1.88}\text{Sr}_{0.12}\text{CuO}_4$ . *Phys. Rev. B* **90**, 100510 (2014).
- [59] Tranquada, J. M. Cuprate superconductors as viewed through a striped lens. *Advances in Physics* **69**, 437-509 (2021).

## **Data availability**

All data that support the plots and other findings of this study are available from the corresponding authors upon reasonable request.

## **Acknowledgements**

We thank John M. Tranquada, Peter Abbamonte, and David Hawthorn for insightful discussions and T. Masuda, S. Asai, and M. Ohkawara for supporting the neutron measurements at HER and TOPAN. All soft X-ray experiments were carried out at the SSRL (beamline 13-3), SLAC National Accelerator Laboratory, supported by the U.S. Department of Energy, Office of Science, Office of Basic Energy Sciences under Contract No. DE-AC02-76SF00515. The neutron scattering experiments were performed under the Joint-Use Research Program for Neutron Scattering, Institute for Solid State Physics, University of Tokyo, at the Japan Research Reactor JRR-3 (Program Nos. 21527 and 22402). We acknowledge the support from Center of Neutron Science for Advanced Materials, Institute for Materials Research, Tohoku University. S.A.K. acknowledges the support by Department of Energy, Office of Basic Energy Sciences, under contract no. DE-AC02-76SF00515 at Stanford. M.F. is supported by Grant-in-Aid for Scientific Research(S) (GrantNo.21H04987).

## **Author contributions**

J.-S.L. and C.-C.K carried out the RSXS experiment and analyzed the data. T.W. Y.I., T.T., and M.F. synthesized the materials and carried out the neutron scattering. S.A.K., C.-C.K., and J.-S.L. wrote the manuscript with input from all authors. J.-S.L. coordinated the project.

## **Competing interests**

The authors declare no competing interests.

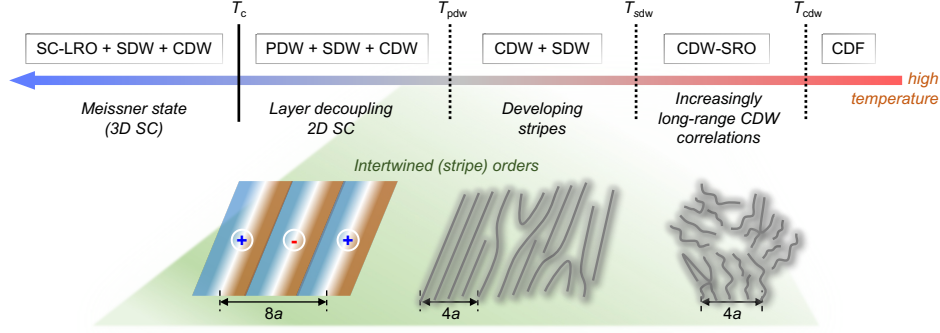


FIG. 1. **Evolution of intertwined orders.** A peak in the charge-density structure factor – generally identified with fluctuating CDW order (CDF) – is detectable up to relatively high temperatures [52]. With decreasing temperature, CDW-SRO grows significantly stronger below a crossover temperature,  $T_{cdw}$ , which is greater than or equal to the temperature,  $T_{sdw}$ , below which unidirectional SDW (stripe) order onsets. We associate the onset of PDW order with the temperature  $T_{pdw} \leq T_{sdw}$  at which the in-plane resistivity, but not the interplane resistivity, drops precipitously, indicative of 2D SC. The 3D SC (Meissner) state, which exhibits perfect diamagnetism and in which all components of the resistivity vanish, appears below a much suppressed  $T_c$ . The 1Q peak is detected at temperatures roughly midway between  $T_{pdw}$  and  $T_c$ , where it is plausible that some degree of PDW and uniform (long-range-order, LRO) SC (possibly fluctuating) orders coexist. The cartoon below represents a real-space visualization of the nature of the intertwined orders in various ranges of  $T$ . It is plausible that the states with coexisting orders are inhomogeneous, but as long as the resulting domains in which one or another order dominates are sufficiently small and the orders overlap in significant interfacial regimes, this does not qualitatively change the analysis.

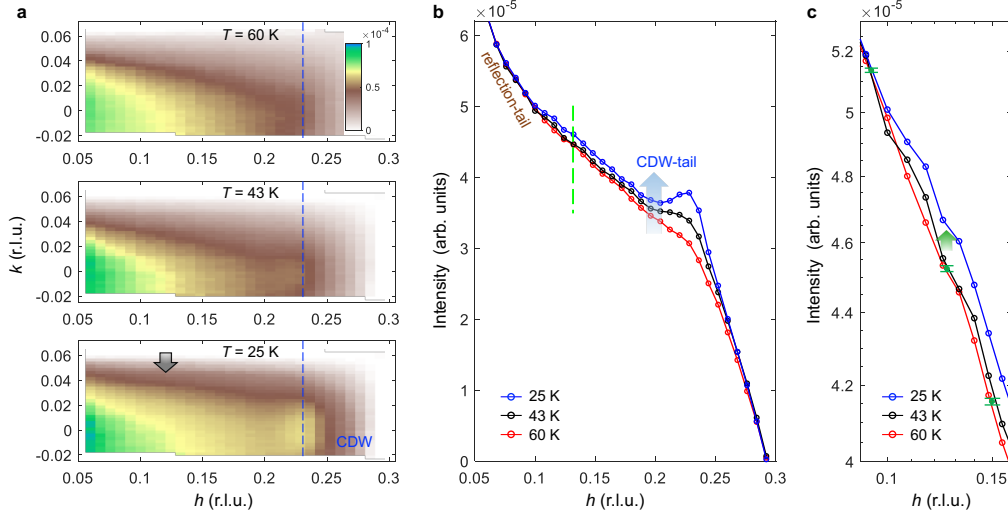


FIG. 2. **Cu  $L$ -edge resonant x-ray scattering on Fe-doped LSCO.** **a**, RSXS maps at temperatures of  $T = 60$  K (top-panel),  $43$  K (middle), and  $25$  K, below  $T_{\text{pdw}} = 32$  K, (bottom), respectively. All data were collected with the detector at an angle of  $106^\circ$ . The dashed lines indicate the CDW order at  $\vec{K}$ . The gray-colored arrow in data at  $T = 25$  K denotes an excess of intensity distribution around  $\vec{K}/2$ . **b**,  $h$ -scan projected along the  $k$ -direction in RSXS maps measured at each temperature shown in (a). With decreasing the sample temperature, CDW order are enhanced. The blue-colored arrow indicates the increase in CDW background with increasing CDW order, while the reflection tail, comes from a  $h \sim 0$ , remains temperature independent. The green-colored dashed line marks the putative 1Q peak. **c**, The extended  $h$ -scan for potential subharmonic order area (i.e., around  $\vec{K}/2$ ). The green-colored arrow indicates the intensity increment at  $T = 25$  K, compared to  $T = 60$  K and  $43$  K. The green circles with the cap-bar denote the statistic error between  $T = 60$  K and  $43$  K. based on the 1 standard deviation (1 SD)



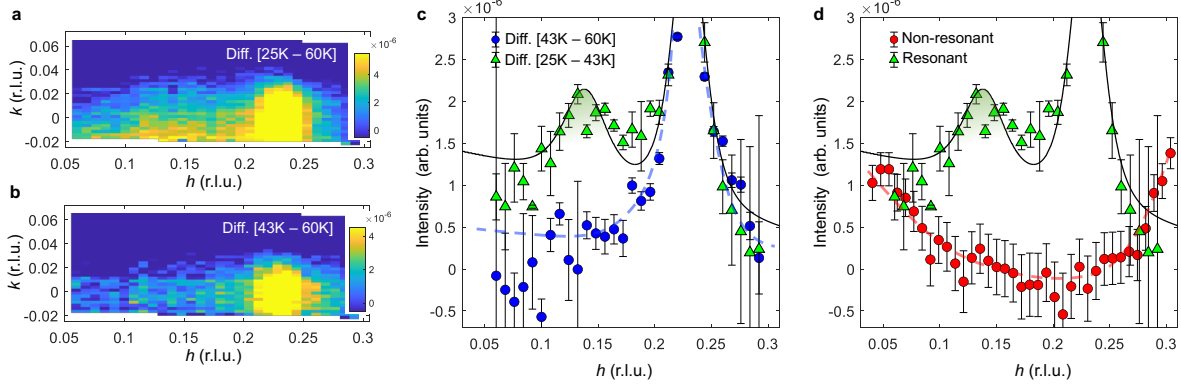


FIG. 3. **A signature of the putative 1Q peak in Fe-doped LSCO.** **a,b**, Differences between RSXS maps measured at 25 K, 43 K, and 60 K. **c**, Comparison of  $h$ -scans projected along the  $k$ -direction, which were extracted from difference maps ( $I_{25\text{K}} - I_{43\text{K}}$ , below  $T_{\text{pdw}}$ ) and ( $I_{43\text{K}} - I_{60\text{K}}$ , above  $T_{\text{pdw}}$ ). The solid line represents the fitting result, while dashed lines and shading serve as visual guides. All error bars denote the statistical error, including the experimental resolutions. **d**, Comparison of differences extracted below and above Cu  $L$ -edge resonant photon energy (933.1 eV). The red dashed line and shade are guides to the eye.

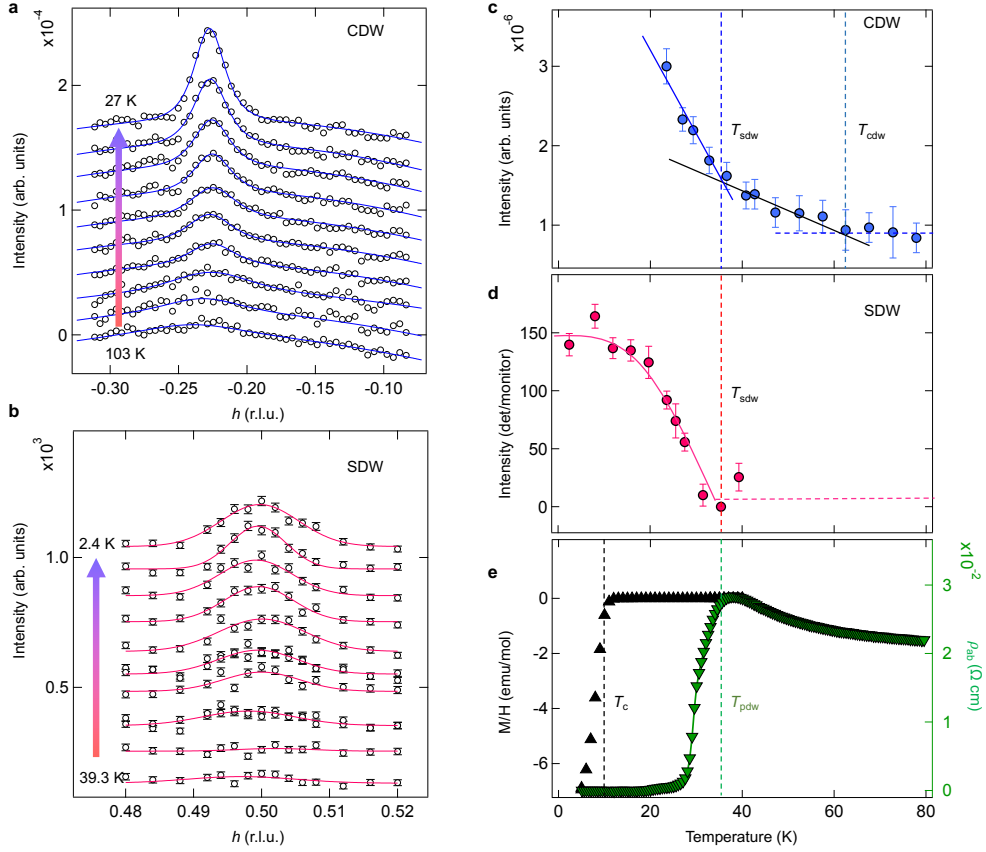


FIG. 4. **DWs and superconducting properties on Sr-doped LBCO.** **a,b** Intensity profiles of CDW measured at  $q = (h, 0, \sim 1.5)$  through RSXS and SDW measured at  $q = (h, 0.622, 0)$  through neutron scattering as a function of temperature, respectively. The solid lines are Lorentzian fits. The error bars represent 1 SD of the fit parameters. **c,d**, Integrated intensity plots by using the fitted CDW and SDW results, respectively. All dashed and solid lines are guides to the eye. **e**, Superconductivity measurements as a function of temperature. Magnetic susceptibility for bulk superconductivity (left  $y$ -axis). The zero-field resistivity ( $\rho_{ab}$ ) along the in-plane (right  $y$ -axis).

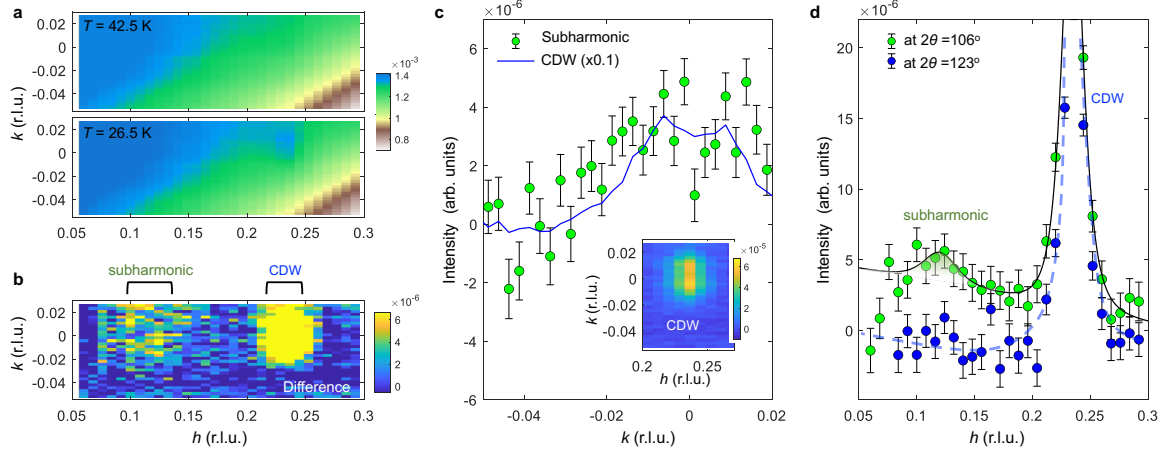


FIG. 5. **Cu  $L$ -edge resonant x-ray scattering on Sr-doped LBCO.** **a**, RSXS maps at  $T = 42.5$  K (upper panel) and  $26.5$  K (lower panel). **b**, Difference map between the two temperatures ( $26.5$  K and  $42.5$  K, below  $T_{\text{pdw}}$ ). The brackets indicate the positions of the CDW and subharmonic. **c**,  $k$ -scans intensity integrated at the fixed regions,  $0.10 < h < 0.15$  r.l.u. (indicating the subharmonic area) and  $0.21 < h < 0.26$  r.l.u. (CDW area). The line and circled date correspond to the subharmonic and CDW regions, respectively. The inset shows the extended CDW region. **d**, Intensity of  $h$ -scans (green-colored circles) integrated over the  $k$ -direction in the difference RSXS map. The data marked by the blue-colored circles shows a different two-theta (detector angle,  $2\theta = 123^\circ$ ), where  $l$  vector at  $\vec{Q}$  is  $\sim 1.7$  r.l.u. Whereas, the green-colored circles were measured at  $2\theta = 106^\circ$ ,  $l \sim 1.5$  r.l.u. The solid line represents the fitting result, while dashed lines and shading serve as visual guides.

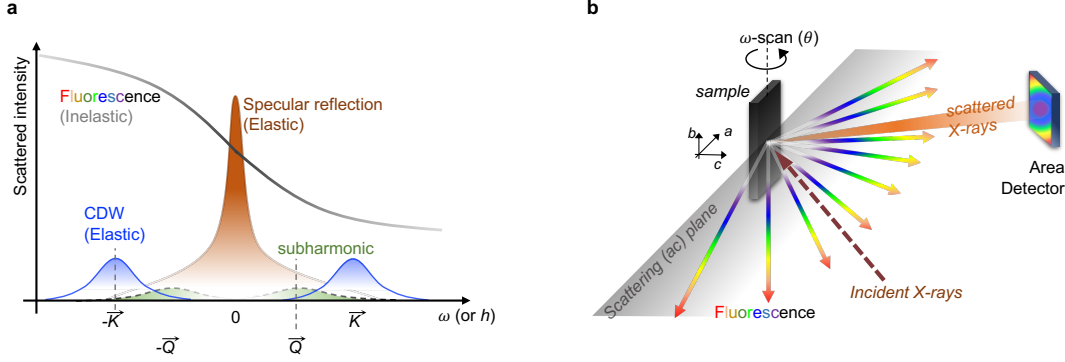


FIG. – **Extended data 1. Background issue in x-ray scattering measurement.** **a**, Massive backgrounds at the expected subharmonic positions ( $\vec{Q}$  and  $-\vec{Q}$ ). There are three dominant components – 1) a scattering intensity from specular (elastic) reflection of the sample surface (i.e., from  $h = 0$ ), 2) fluorescence (inelastic) contribution, and 3) another elastic signal from the CDW stripe (i.e., from  $\vec{K}$  and  $-\vec{K}$ ). The 1) and 2) components are expected to be largely independent of temperature. The 3) component has a temperature dependence. **b**, Schematic carton for our RSXS experimental configuration. The scattering plane is  $ac$ -plane. While rotating the sample angle ( $\theta$ ), the so-called  $\omega$ -scan, the RSXS intensity is accumulated at a fixed detector angle ( $2\theta$ ). Due to the resonant nature, the scattered x-rays include not only the elastic component (e.g., DWs and specular) but also the inelastic component (e.g., fluorescence).

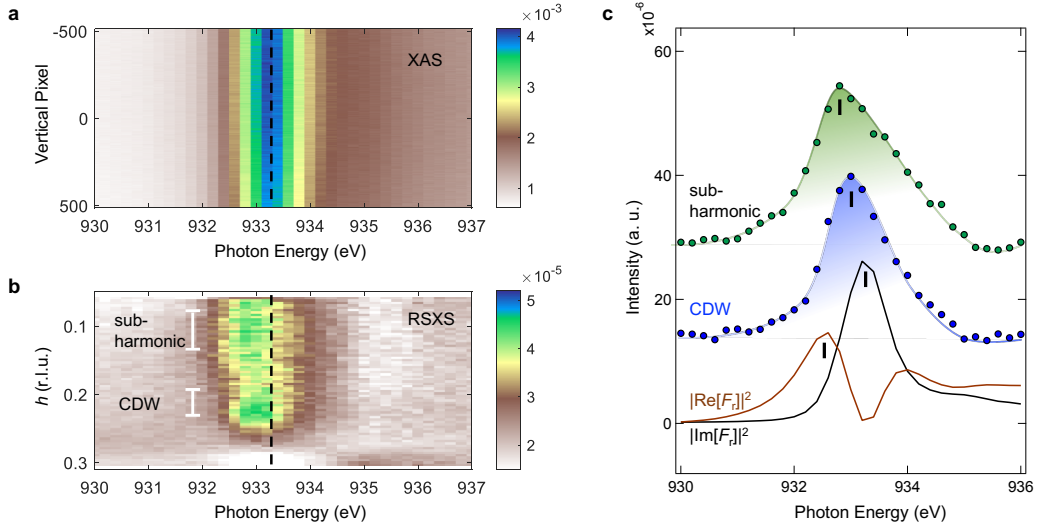


FIG. – **Extended data 2. Resonant profile on Fe-doped LSCO.** **a**, X-ray absorption spectroscopy (XAS) from the sample. It becomes a source of fluorescence background discussed in Extended Data Fig. 1. The dashed line denotes the absorption maximum. **b**, Incident photon energy vs.  $h$ . At slightly lower energy than the absorption maximum, both the CDW and subharmonic orders are resonated. **c**, Projected intensity from the map regarding both subharmonic (green colored) and CDW (green colored) areas where are from two  $h$  regions marked in the Extended Data Fig. 2b.  $\text{Im}[F_r]$  is XAS, and  $\text{Re}[F_r]$  is a result driven by Kramers-Kronig relation (KKR) of  $\text{Im}[F_r]$  term, which is related with the electron density (i.e., charge contribution). The resonant x-ray scattering signal is related with a combination of both terms,  $\text{Re}[F_r]$  and  $\text{Im}[F_r]$ . The observed DWs signals tend to move to the lower energy side compared to the electron absorption energy.

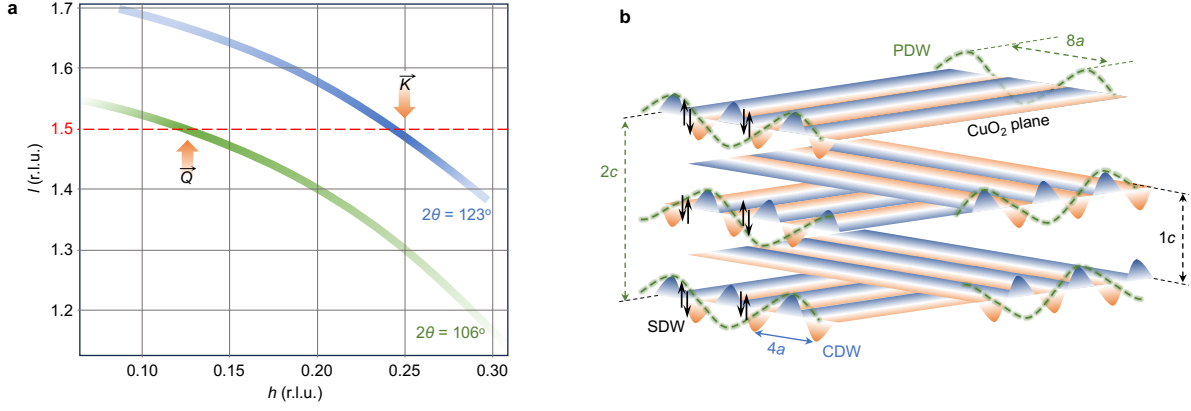


FIG. – **Extended data 3. Understanding  $q$ -space and real-space.** **a**, The  $h/l$ -vectors trajectory through an  $\omega$ -scan at the fixed detector angle ( $2\theta$ ). The blue trajectory ( $2\theta = 123^\circ$ ) represents the CDW (i.e.,  $\vec{K}$ ) optimized at  $l \sim 1.5$  r.l.u., while the green trajectory ( $2\theta = 106^\circ$ ) represents the 1Q peak (i.e.,  $\vec{Q}$ ) also optimized at  $l \sim 1.5$  r.l.u. **b**, Schematic cartoon illustrating the suggestive stripes image in real-space. Within each  $\text{CuO}_2$  plane, a CDW forms with  $4a$  periodicity. The SDW (i.e., Néel antiferromagnetic order) is separated by a periodic array of anti-phase boundaries where the density of doped holes is maximal. With intertwined DWs, the PDW order is expected to be shifted by half a period relative to the SDW order, resulting in an  $8a$  periodicity. Along the  $c$ -axis, the inter  $\text{CuO}_2$  planes form the  $90^\circ$  rotation, representing “layer-decoupling.” With a double unit-cell along the  $c$ -direction (i.e.,  $2c$ ), the same wave pattern emerges.